Heliyon 10 (2024) e32573

Contents lists available at ScienceDirect

Heliyon

journal homepage: www.cell.com/heliyon

Research article

Unexpected discovery: "A new 3,3′-bipyrazolo[3,4-*b*]pyridine scaffold and its comprehensive analysis"

Efraín Polo-Cuadrado [a], Karoll Ferrer [b,*], Jesús Sánchez-Márquez [c], Andrés Charris-Molina [d], Yeray A. Rodríguez-Núñez [e], Luis Espinoza-Catalán [f], Margarita Gutiérrez [g,**]

[a] *Departamento de Química Orgánica, Facultad de Ciencias Químicas, Universidad de Concepción, Concepción, Chile*
[b] *Laboratory of Growth Regulators, Institute of Experimental Botany, The Czech Academy of Sciences, Palacký University, Šlechtitelů 27, 78371 Olomouc, Czech Republic*
[c] *Departamento de Química-Física, Universidad de Cádiz, Facultad de Ciencias, 4011510 Puerto Real, Cádiz, Spain*
[d] *CIBION-CONICET, Centro de Investigaciones en Bionanociencias, NMR Group, Polo Científico Tecnológico, Ciudad Autónoma de Buenos Aires, Buenos Aires C1425FQD, Argentina*
[e] *Laboratorio de Síntesis Orgánica y Organometálica, Centro de Química Teórica y Computacional (CQTC), Universidad Andrés Bello, Facultad de Ciencias Exactas, Santiago 8370146, Chile*
[f] *Departamento de Química, Universidad Técnica Federico Santa María, Av. España No. 1680, Valparaíso 2340000, Chile*
[g] *Laboratorio Síntesis Orgánica y Actividad Biológica (LSO-Act-Bio), Instituto de Química de Recursos Naturales, Universidad de Talca, Casilla 747, Talca 3460000, Chile*

ARTICLE INFO

Keywords:
Pyrazolo[3,4-*b*]pyridine
Vilsmeier-haack reaction
Acetamidopyrazoles
Ab initio calculation

ABSTRACT

In this study, a novel 3,3′-bipyrazolo [3,4-*b*]pyridine-type structure was synthesized from 5-acetylamino-3-methyl-1-phenylpyrazole using the Vilsmeier-Haack reaction as a key step. The spectroscopic properties and structural elucidation of the compound were determined with the use of FT-IR, HRMS, ^{1}H NMR, and ^{13}C NMR. Likewise, the theoretical analysis of the IR and NMR spectra allowed peaks to be assigned and a solid correlation was demonstrated between the experimental and theoretical results. Finally, ab initio calculations based on the density functional theory method at the B3LYP/6-311G (d,p) level of theory were used to determine the conformational energy barrier, facilitating the identification of the most probable conformers of the synthesized compound. Overall, our findings contribute to the understanding of bipyrazolo [3,4-*b*]pyridine derivatives.

1. Introduction

Pyrazolo [3,4-*b*]pyridine derivatives exhibit promising pharmacological activities, making them attractive candidates for drug development. These compounds have been explored for their potential in various therapeutic applications, including cancer [1], inflammation [2], neurological disorders [3], infectious diseases [4], and cardiovascular conditions [5]. The unique structural features of pyrazolo [3,4-*b*]pyridine derivatives contribute to their interactions with specific biological targets, leading to the discovery of novel drug candidates [6]. Additionally, owing to their unique luminescent properties [7,8], pyrazolo [3,4-*b*]pyridine scaffolds can be

* Corresponding author.
** Corresponding author.
E-mail addresses: karoll.ferrerpertuz@upol.cz (K. Ferrer), mgutierrez@utalca.cl (M. Gutiérrez).

https://doi.org/10.1016/j.heliyon.2024.e32573
Received 8 December 2023; Received in revised form 13 May 2024; Accepted 5 June 2024
Available online 6 June 2024

exploited for biosensing applications [9–11].

Due to the importance of pyrazolo [3,4-*b*]pyridine derivatives as substructures in drug design, many efforts have been devoted to the development of effective protocols for their preparation. The methods for obtaining this nucleus can be summarized into two strategies: forming a pyridine ring into an existing pyrazole ring and forming a pyrazole ring into a preexisting pyridine ring [12].

Vilsmeier–Haack reaction carried out on acetamidopyrazoles can form a series of fused structures pyrazolo-pyridine, which are valuable precursors in the construction of different heterocyclic compounds through various transformations, such as nucleophilic addition reactions, condensations, or reductions, resulting in the formation of diverse products with enhanced complexity. In particular, the reaction of 5-acetylamino-3-methyl-1-phenylpyrazole **2** under Vilsmeier-Haack reaction conditions produces mostly 6-chloro-3-methyl-1-phenyl-1*H*-pyrazolo [3,4-*b*]pyridine-5-carbaldehyde **3**, in addition to the formation of a chlorinated product (6-chloro-3-methyl-1-phenyl-1*H*-pyrazolo [3,4-*b*]pyridine) **4** in small quantities [13] (Scheme 1).

Continuing our ongoing interest in bioactive nitrogen-containing heterocycles, we directed our attention towards the synthesis of 5-carbaldehyde **3**. However, upon purifying the reaction mixture and performing NMR analysis, compound **3** was not obtained; instead, compound **5** was formed. Herein, we present the data and results utilized to confirm the structure of the novel 3,3′-bipyrazolo [3,4-*b*] pyridine scaffold **5** (Fig. 1).

In addition to employing FT-IR, HRMS, and NMR experimental techniques, the conformational barrier of the obtained compound was also studied. The most likely conformers of bipyrazolo [3,4-*b*]pyridine **5** were identified, and the theoretical IR and NMR spectra were generated for comparison with the corresponding experimental spectra.

2. Experimental

2.1. Materials and methods

1D and 2D NMR spectra (400 MHz for protons and 100 MHz for carbon) were recorded on an AM-400 spectrometer (Bruker, Rheinstetten, Germany) using $CDCl_3$ as the solvent. Tetramethylsilane (TMS) was used as an internal standard. IR spectra (KBr pellets, 500–4000 cm^{-1}) were recorded using a NEXUS 670 FT-IR spectrophotometer (Thermo Nicolet, Madison, WI, USA). High-resolution mass spectrometry (HRMS) analyses were carried out using a Bruker "Compact" quadrupole time-of-flight mass spectrometry (qTOF-MS, Germany) coupled with an Apollo II ion funnel electrospray ionization (ESI) source. The melting point (m.p.) was determined using an Electrothermal IA9100 apparatus (Stone, Staffs, UK) and was uncorrected. The reaction progress was monitored by thin-layer chromatography (TLC) using Kieselgel 60 F254 plates (Merck). All chemical reagents were of analytical grade, obtained from commercial suppliers, and used without further purification.

2.2. Synthesis of 3,3′-dimethyl-1,1′-diphenyl-1H,1′H-[6,6′-bipyrazolo [3,4-b]pyridine]-5-carbaldehyde 5

A mixture of 5-amino-3-methyl-1-phenylpyrazole **1** (1 g, 5.8 mmol) and an AcOH/Ac_2O mixture (10 mL) was refluxed for 3 h. The reaction mixture was cooled, and the obtained solid was filtered off and recrystallized from EtOH to give 1.1 g of compound **2** (88 %) as white crystals. Acetamide **2** (0.9902 g, 4.6 mmol) was dissolved in DMF (5.0 mL) and the solution was cooled to 0 °C. $POCl_3$ (2.58 mL, 6 mmol) was added slowly under intensive stirring at 0 °C. The reaction mixture was allowed to reach room temperature and then, was refluxed for 8 h at 80 °C. After the completion of the reaction, the mixture was cooled and neutralized with saturated aq. NaOAc solution. The resulting reaction mixture was extracted with EtOAc (20 mL), washed with water (100 mL), and dried over anhydrous Na_2SO_4. The solvent was evaporated and the crude material was purified by column chromatography (30 % EtOAc/hexane) to obtain pure product **5** (40 %) as a white solid; m. p. = 182–184 °C; IR (ν_{max}, KBr, cm^{-1}): 3050 (CH arom.), 2990 (CH aliph.), 1690 (CO); ^1H NMR ($CDCl_3$, 400 MHz) δ_H (ppm): 2.68 (s, 3H, CH_3), 2.72 (s, 3H, CH_3), 7.22 (d, J = 8.3 Hz, 1H, CH-pyridine), 7.36 (t, J = 7.4 Hz, 1H, ArH), 7.42 (t, J = 7.4 Hz, 1H, ArH), 7.59 (m, 4H, ArH), 8.00 (d, J = 8.3 Hz, 1H, CH-pyridine), 8.27 (dd, J = 8.2, 2.3 Hz, 4H, ArH), 8.67 (s, 1H, CH-pyridine), 10.55 (s, 1H, CHO). ^{13}C NMR ($CDCl_3$, 101 MHz) δ_C (ppm): 12.4 (CH_3), 12.4 (CH_3), 115.6(C), 116.6 (C), 117.4 (CH), 120.6 (2 x CH), 120.9 (2 x CH), 122.8 (C), 125.8 (CH), 126.6 (CH), 129.0 (2 x CH), 129.2 (2 x CH), 131.4 (CH), 132.7 (CH), 138.3 (C), 139.0 (C), 142.7 (C), 145.5 (C), 149.5 (C), 149.9 (C), 150.7 (C), 152.8 (C), 188.7 (C═O). HRMS (ESI, m/z): $C_{13}H_3N_6$ [M–2 ($^{\cdot}C_6H_5$)-(CH_4)–CHO + H]$^{2.+}$ 243.0414 found 243.7811 (base ion).

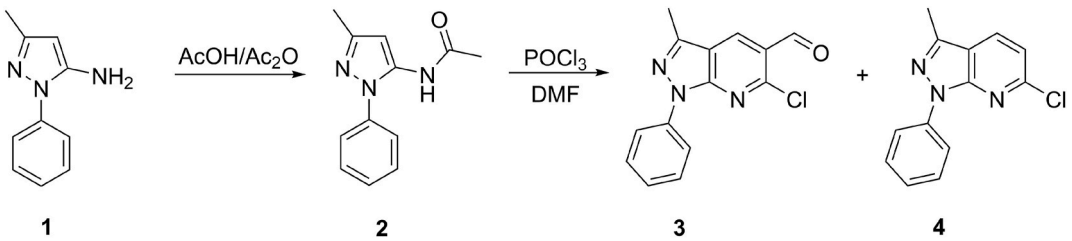

Scheme 1. 5-acetylamino-3-methyl-1-phenylpyrazole (**2**) under Vilsmeier-Haack reaction conditions.

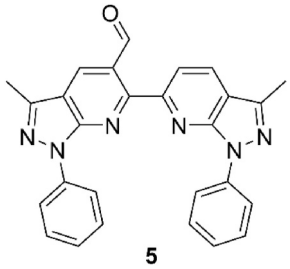

Fig. 1. 3,3′-dimethyl-1,1′-diphenyl-1H,1′H-[6,6′-bipyrazolo [3,4-*b*]pyridine]-5-carbaldehyde **5**.

3. Computational methods

3.1. Theoretical calculations

To calculate the conformational barrier, the energy values for the curve were computed using the B3LYP hybrid density functional [14,15] and 6-311G (d,p) basis set [16,17]. Subsequently, the points on the curve corresponding to the maxima or minima (eight structures) were optimized at the B3LYP/6-311 + G (2d,p) level of calculation [18]. The energy was then determined using the CAM-B3LYP method/basis set (Handy and coworkers' long-range-corrected version of B3LYP using the Coulomb-attenuating method)/aug-cc-pVTZ [19,20] on the geometry obtained with B3LYP/6-311 + G (2d,p).

For calculating vibrational frequencies, the B3LYP/6-311 + G (2d,p) method/basis-set was employed for previously optimized structures using the same method/basis-set. Chloroform solvent effects were considered using the integral equation formalism polarizable continuum model (IEFPCM) [21–23]. The scheme used to organize this analysis was consistent with employed in Ref. [23].

The theoretical NMR values were obtained using the Gauge-Independent Atomic Orbital (GIAO) method [24–27] in conjunction with the B3LYP/6-311 + G (2d,p) method/basis-set. The scheme used to organize this analysis was the same as that employed in Refs. [28–30].

4. Results and discussion

4.1. Synthesis and characterization

The starting compound, 5-acetylamino-3-methyl-1-phenylpyrazole **2**, was synthesized via conventional methods, as reported in the literature [31], involving the reaction of 5-amino-3-methyl-1-phenylpyrazole **1** with an AcOH/Ac_2O mixture. The bipyrazolo [3,4-*b*] pyridine **5** derivative was obtained by the reaction of 5-acetylamino-3-methyl-1-phenylpyrazole **2** with Vilsmeier-Haack reagent (Scheme 2).

The structure of compound **5** was supported by findings derived from ^{1}H NMR, ^{13}C NMR, IR, and HRMS (Fig. 2). The IR spectrum of the synthesized bipyrazolopyridine showed the presence of absorption bands at 3050 and 2990 cm^{-1}, due to aromatic and aliphatic C–H stretching vibrations, and a strong absorption band at 1690 cm^{-1}, corresponding to the C═O group frequency (see Figs. SI–8).

^{1}H and ^{13}C NMR assignments were completed using 1D and 2D heteronuclear correlation HSQC and HMBC techniques (Fig. 3). The ^{1}H NMR spectrum (Figs. SI–1) was characterized by the presence of three groups of signals (aliphatic protons, aromatic protons, and protons near heteroatoms).

The observed signals in the ^{1}H NMR spectrum at $\delta_H = 2.72$ ppm (3H, s) and 2.68 (3H, s) were attributed to methyl groups CH_3-3 and CH_3-3′, respectively. In the ^{13}C NMR spectrum, the carbons $\underline{C}H_3$-3 and $\underline{C}H_3$-3′ appeared at $\delta_C = 12.49$ and 12.42 ppm, respectively. The assignments for these signals were confirmed using 2D HSQC spectra (see Figs. S4 and S5). Further evidence was obtained from the 2D HMBC spectrum (Figs. S6 and S7), which showed two important correlated couplings (Fig. 4B). The first coupling was between protons CH_3-3 (^{1}H, at 2.72 ppm) and C-3 (^{13}C, 145.54 ppm) and C-3a (^{13}C, 116.64 ppm), while the second coupling was between protons CH_3-3' (^{1}H, at 2.68 ppm) and C-3' (^{13}C, 142.73 ppm) and C-3a' (^{13}C, 115.61 ppm).

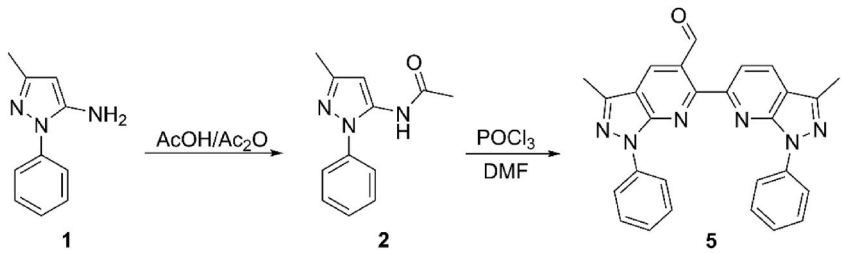

Scheme 2. Synthesis of the bipyrazolo [3,4-*b*]pyridine derivative **9** from **2**.

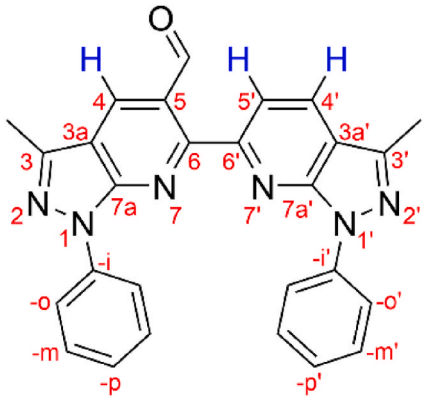

Fig. 2. The numbering system of 3,3′-dimethyl-1,1′-diphenyl-1H,1′H-[6,6′-bipyrazolo [3,4-*b*]pyridine]-5-carbaldehyde **5**.

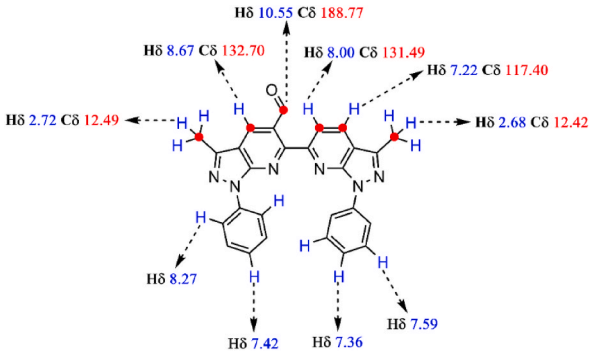

Fig. 3. ^{1}H and ^{13}C NMR chemical shifts of bipyrazolo [3,4-*b*]pyridine **5**.

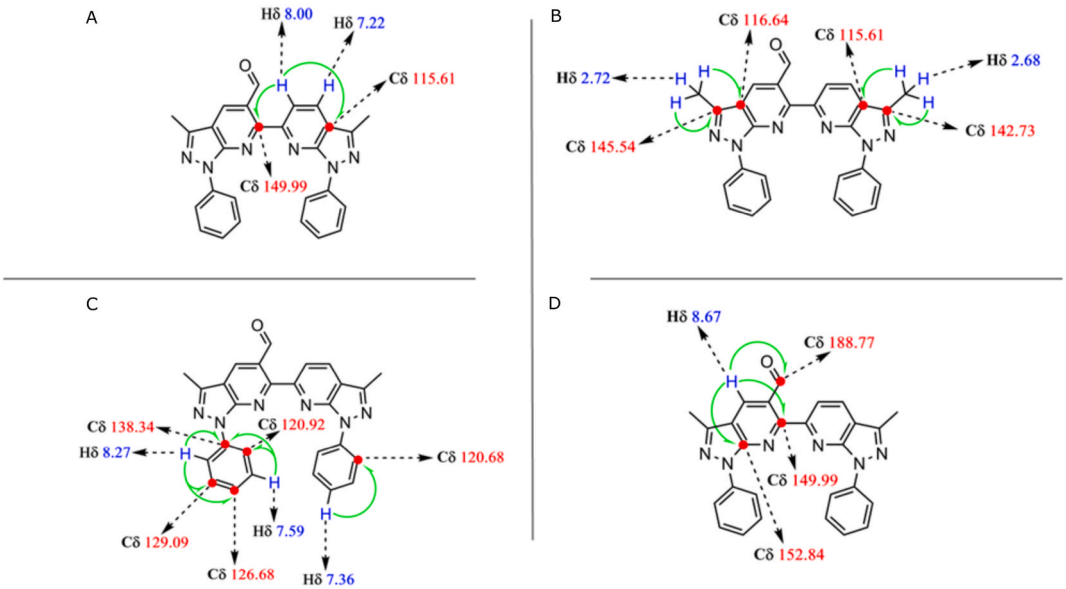

Fig. 4. HMBC correlations of bipyrazolo [3,4-*b*]pyridine **5**.

The presence of aromatic signals at $\delta_H = 8.27$ ppm (4H, dd, $J = 8.2$, 2.3 Hz, ArH-*o* and -*o'*), 7.59 ppm (4H, m, ArH-*m* and -*m'*), 7.42 ppm (1H,t, $J = 7.4$ Hz, ArH-*p*) and 7.36 ppm (1H, t, $J = 7.4$ Hz, ArH-*p'*) were assigned to the hydrogens -*o*, -*m*, and -*p* in both aromatic systems, respectively. In the ^{13}C NMR spectrum (see Figs. S2 and S3), the observed signals at $\delta_C = 129.23$ (2 x CH), 129.09 (2 x CH),

126.68 (CH), 125.88 (CH), 120.93 (2 x CH), and 120.68 (2 x CH) ppm were assigned to the aromatic carbons *–m'*, *-m*, *-p*, *-p'*, *-o* and *–o'*, respectively. The assignment of these signals was confirmed by 2D HSQC and HMBC spectra (Fig. 4C).

The most valuable information regarding the structure of bipyrazolo [3,4-*b*]pyridine was obtained from the proton resonance of pyridine rings at 8.67 ppm (1H, s), 8.00 (1H, d, $J = 8.3$ Hz, 1H), and 7.22 (1H, d, $J = 8.3$ Hz) corresponding to the H-4, H-5′, and H-4′ protons, respectively. Additionally, the 2D HSQC spectrum provided essential data for the assignment of carbons C-4, C-5′, and C-4' appearing at $\delta_C = 132.70$, 131.49, and 117.40 ppm, respectively. In the ^{1}H NMR spectrum, a singlet at 10.55 ppm (1H, s) was observed, attributed to the –CHO proton. The ^{13}C NMR spectrum showed the carbonyl group at $\delta_C = 188.77$ ppm, supported by the HMBC correlation (Fig. 4D).

Additional assignments were obtained from the HMBC spectra (Table S1). The H-4 signal (^{1}H, 8.67 ppm) displayed correlations with C-7a (13C, 152.84 ppm), C-6 (13C, 149.99 ppm), and CHO (^{13}C, 188.77 ppm) (Fig. 4D). The H-5′ signal (^{1}H, at 8.00 ppm) exhibited and HMBC correlation with both C-6 (^{13}C, 149.99 ppm) and C-3a' (^{13}C, 115.61 ppm) (Fig. 4A).

Compound **5** (mass exact = 444.1699) was analyzed by stepwise mass spectrometric fragmentation experiments in positive ionization mode (see Supporting Information Fig. S14). Scheme 3 depicts the fragmentation pathway of **5** and the postulated fragment ion structures.

Novel 3,3′-bipyrazolo [3,4-*b*]pyridine scaffold **5** was obtained from intermediates **8** and **9**, contrary to what has been proposed by other authors [32] who suggest that similar formylation should lead to compounds **3** and **4** shown in Scheme 1. Thus, intermediate **8** would lead to compound **3** while intermediate **9** to compound **4**. However, what occurred was the interaction of these two intermediates to generate compound **5**, as outlined in Scheme 4 as plausible mechanism.

The reaction involves the use of Vilsmeier's reagent (VR), consisting of a dimethylformamide (DMF), and phosphoryl chloride ($POCl_3$) mixture. A plausible mechanism proceeds via formylation of 5-acetylamino-3-methyl-1-phenylpyrazole **2** to generate intermediate **6**. This entails the attack of the carbon 3 of the amino pyrazole **2** by VR. Then, a new VR molecule is attacked, but this time by the oxygen of the amide leading to the formation of **7**. The mechanism bifurcates into two pathways to form intermediates **8** and **9** from **7**. The pathway for the formation of intermediate **8** is shown with red arrows representing specific electronic movements for its generation, as well as the formation of intermediate **9** (depicted with blue arrows). Subsequently, a nucleophilic attack from intermediate **8** to **9** occurs, leading to the formation of **10**, which then undergoes a transposition for stability to generate intermediate **11**. Consequently, in intermediate **11**, there is an elimination of HCl along with water attacking the iminic carbon, and eliminations of trimethylamine occur to generate the unexpected bipyrazolo [3,4-*b*]pyridine **5.**

5. Theoretical details

5.1. Structural optimization. Conformational barrier

In this section, the most probable conformers of bipyrazolo [3,4-*b*]pyridine **5** are determined by studying the torsion of its characteristic dihedral angle. After determining the conformational energy barrier, the most probable structures were qualitatively estimated and refined at a higher calculation level. Fig. 5-A displays the conformational energy curve of bipyrazolo [3,4-*b*]pyridine, while Fig. 5-B illustrates the rotation of the dihedral angle to obtain points on curve A. As depicted, the curve shows four relative minima (marked as 1–4) corresponding to dihedral angles of 146.8, 206.8, 304.3, and 409.3°, respectively. Additionally, four relative maxima (labeled A-D) corresponding to dihedral angles of 86.8, 191.8, 274.3, and 379.3°, respectively, are also visible. These eight structures are shown in Figs. S9 and S10 of the Supporting Information.

Fig. 6 depicts the energy profile of bipyrazolo [3,4-*b*]pyridine (main structures from Fig. 5-A), and it is like Fig. 5-A with the distinction that only the important structures, the maxima, and the minima are depicted, aiming to obtain the values of the energy

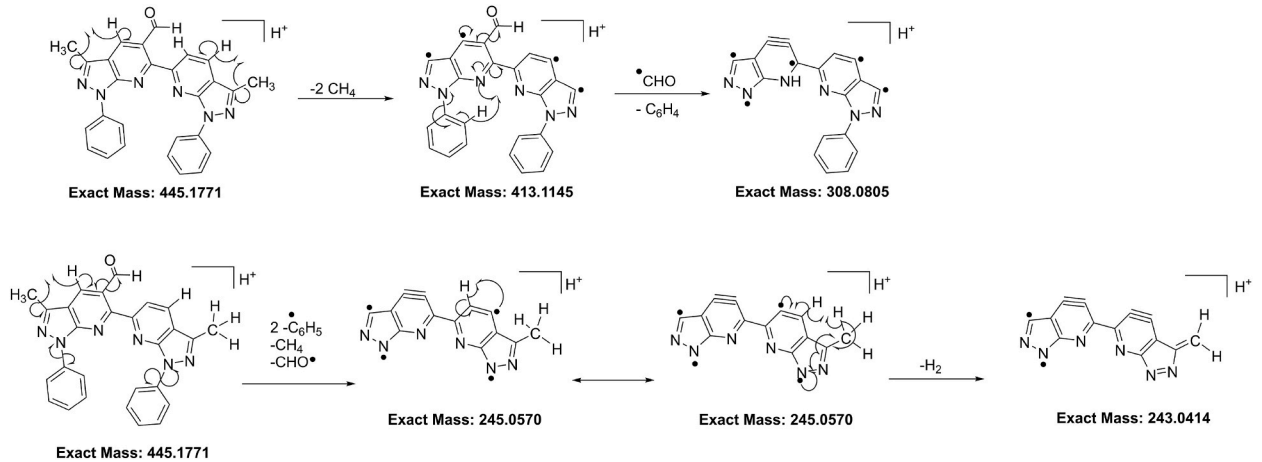

Scheme 3. Possible fragmentation pathways for compound **5**.

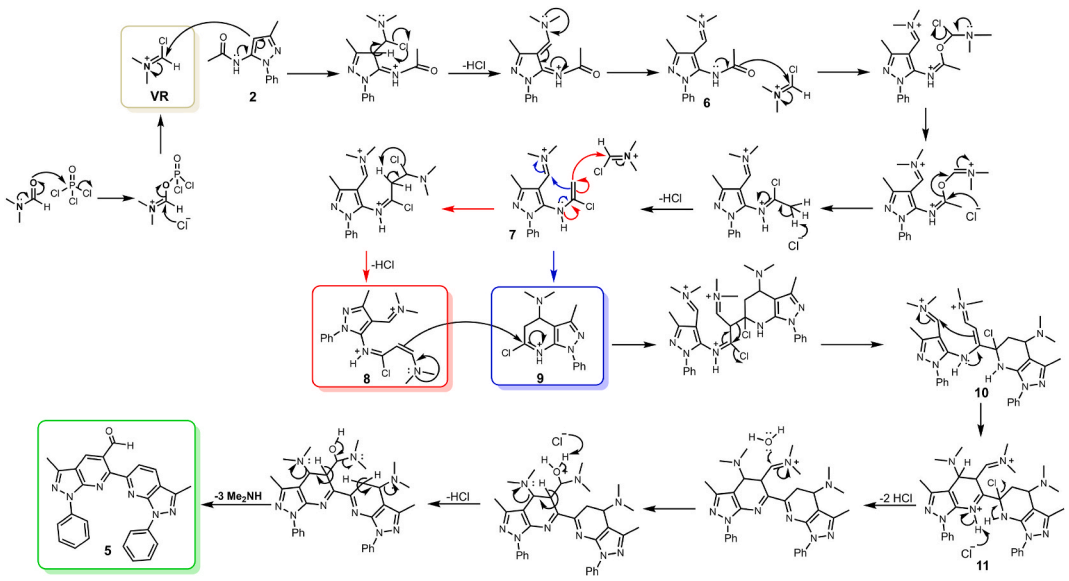

Scheme 4. A plausible mechanism for the formation of bipyrazolo [3,4-*b*]pyridine **5**.

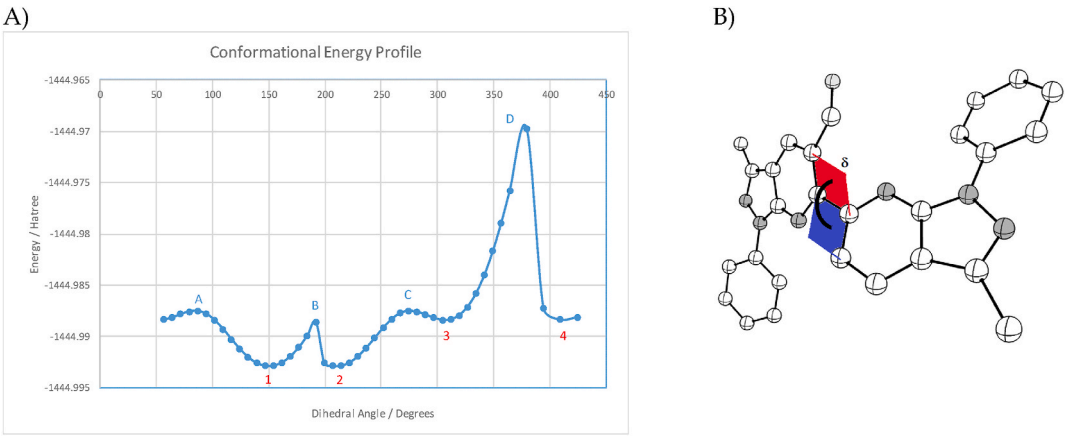

Fig. 5. A) Conformational energy profile of bipyrazolo [3,4-b]pyridine. The points on the curve were obtained at the B3LYP/6-311G (d,p) level. B) Dihedral angle rotated to obtain points on curve A.

barriers. These geometries have been refined using a slightly superior methodology compared to that employed to obtain Fig. 5-A. Subsequently, the energies of the key structures (marked as 1–4 and A-D in Fig. 5) have been recalculated using a highly accurate computational approach as discussed in the Theoretical calculations section. The lowest-energy structures, 1 and 2, exhibit identical energy values since they are enantiomers. Hence, the Boltzmann distribution ratio between these two structures is one. In contrast, structure 3, compared to the previous ones, possesses a Boltzmann ratio of 0.01079. Consequently, a significant contribution to the experimental spectra is not expected due to its low population. The outcomes presented in Fig. 5 lead examination of the spectra of structure 1 in the subsequent sections, as the spectra of structure 2 mirror those of 1, and the contributions of structures 3 and 4 are negligible.

5.2. *Theoretical versus experimental IR analysis*

The experimental and theoretical transmittances in the IR spectrum of bipyrazolo [3,4-*b*]pyridine **5** are shown in Fig. 7. This spectrum has been divided into three regions for interpretation purposes. The first region spans from 3200 to 2800 cm^{-1} and includes different C–H stretching vibrations, highlighting the hydrogen stretching of the phenyl group observed at 2921 cm^{-1}. Moving to the second part of the spectrum, ranging from 1800 to 1000 cm^{-1}, several significant peaks of different vibrational modes are observed. At 1680 cm^{-1}, vibrations belonging to the C═O stretching of the carbonyl group are evident, while two other notable peaks (1595 and 1506 cm^{-1}) are associated with multiple bending modes involving many hydrogen atoms. Finally, the spectral range between 900 and

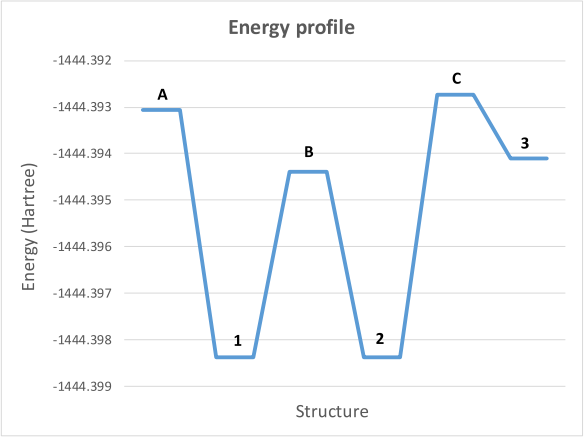

Fig. 6. The energy profile of bipyrazolo [3,4-b]pyridine was calculated using the CAM-B3LYP/aug-ccpVTZ method/basis set on geometries obtained at B3LYP/6-311 + G (2d,p).

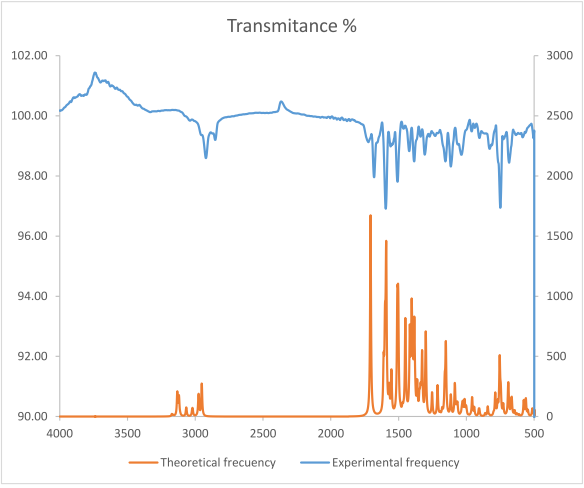

Fig. 7. Comparison of the main frequencies (experimental and theoretical transmittance) in the IR spectrum of bipyrazolo [3,4-*b*]pyridine.

500 cm^{-1} predominantly features medium to low-intensity bands of bending, torsion, and out-of-plane vibrations. The intense peak at 750 cm^{-1} corresponds to the bending of the hydrogen atoms in the phenyl group.

The displacements corresponding to the different vibrational frequencies are shown in Fig. S11 of the Supporting Information. Based on a comparison between theoretical and experimental spectra (Fig. 7), we propose the following assignment for the peaks in the IR spectrum: A (2921 cm^{-1}), hydrogen stretching of the phenyl group in the same plane as the phenyl (see Figs. S11–A); B (2852 cm^{-1}), hydrogen stretching directly bonded to the carbonyl group; C (1680 cm^{-1}), carbonyl group stretching; D (1595 cm^{-1}), multiple bending modes involving a large number of hydrogen atoms (see Figs. S11–D); E (1506 cm^{-1}), multiple bending modes involving a large number of hydrogen atoms (Figs. S11–E); F (1421 cm^{-1}), bending of methyl group hydrogen atoms (see Figs. S11–F); G (1384 cm-^{1}), bending of methyl group hydrogen atoms; H (1305 cm^{-1}), multiple bending modes involving a large number of hydrogen atoms; and I (750 cm^{-1}), bending of phenyl group hydrogen atoms.

5.3. *Comparing theoretical and experimental NMR*

Table S2 shows the theoretical and experimental NMR chemical shifts of the ^{1}H NMR and ^{13}C NMR spectra. As expected, the lowest chemical shift values were observed for the methyl groups at positions 3 and 3', which were 2.68 and 2.72 ppm (2.74 and 2.76 ppm in the theoretical spectrum). On another hand, the highest chemical shift values were obtained for hydrogen atoms near the electronegative atoms, particularly oxygen in the carbonyl group. In this case, the chemical shift of the H of the CO group was 10.55 ppm (10.90 ppm in the theoretical spectrum), while the H at position 4 registered a value of 8.67 ppm (9.18 ppm in the theoretical spectrum).

The carbon atoms at positions p, p', o, o', 4, 3a, and 3a' exhibited chemical shifts of approximately 120 ppm, consistent with the

range for aromatic carbon atoms. The highest chemical shift was obtained for the carbon atom of the carbonyl group, specifically 163 ppm in the observed spectrum (167 ppm in the theoretical spectrum). Additionally, nitrogen atoms induced high chemical shifts in their neighboring carbons 7a and 7a′ due to their electronegativity, yielding values of 152.8 and 150.7 ppm, respectively (155.7 and 155.9 ppm in the theoretical spectrum).

The strong correlation between the theoretical and experimental values ($R^2 = 0.98$, for ^{1}H NMR spectra and 0.93 for ^{13}C NMR spectra, respectively; see Fig. S15 in the Supporting Information) emphasizes the reliability of the peak assignments in Fig. 2 in conjunction with the theoretical results obtained.

6. Conclusions

The reaction between 5-acetylamino-3-methyl-1-phenylpyrazole **2** and the Vilsmeier-Haack reagent yielded bipyrazolopyridine **5**. The structural elucidation of the synthesized compounds was achieved through a comprehensive approach combining experimental techniques such as FT-IR, HRMS, and NMR spectroscopy, along with theoretical calculations performed with various methods. This meticulous analysis unveiled both the identity and structural intricacies of 3,3′-dimethyl-1,1′-diphenyl-1H,1′H-[6,6′-bipyrazolo [3,4-***b***] pyridine]-5-carbaldehyde **5** with precision. This study provides a clearer explanation of the methods used to characterize the synthesized compound and emphasizes the precision achieved in identifying its structure and structural details.

Theoretical study into the conformational barrier identified two highly probable enantiomeric structures, while two additional stable structures exhibiting a minimum conformational energy barrier showed very low Boltzmann ratios, suggesting brief lifetimes and minimal contribution of these compounds.

Comparative analysis of theoretical IR spectra confirmed identical spectra for the enantiomers, aiding in the assignment of main vibrational frequencies to the corresponding functional groups in compound **5**. This comprehensive analysis has provided a detailed examination of the atomic motions associated with the most significant normal modes of vibration.

Theoretical ^{1}H and ^{13}C NMR spectra were generated and compared with experimental spectra, establishing a robust linear correlation, and confirming the reliability of theoretical predictions, confirmed by the R^2 values.

CRediT authorship contribution statement

Efraín Polo-Cuadrado: Writing – original draft, Methodology, Investigation, Formal analysis. **Karoll Ferrer:** Writing – original draft, Investigation, Conceptualization. **Jesús Sánchez-Márquez:** Writing – original draft, Methodology, Formal analysis. **Andrés Charris-Molina:** Writing – review & editing, Conceptualization. **Yeray A. Rodríguez-Núñez:** Writing – review & editing. **Luis Espinoza-Catalán:** Visualization, Conceptualization. **Margarita Gutiérrez:** Writing – original draft, Resources, Project administration.

Declaration of competing interest

The authors declare that they have no known competing financial interests or personal relationships that could have appeared to influence the work reported in this paper.

Acknowledgments

A FONDECYT project N°1200531 supported this research. E.P–C. thanks FONDECYT Post-Doctoral Fellowship No. 3220681. Y.A. R–N thanks FONDECYT project N° 11241068.

Appendix A. Supplementary data

Supplementary data to this article can be found online at https://doi.org/10.1016/j.heliyon.2024.e32573.

References

[1] J. Witherington, V. Bordas, A. Gaiba, N.S. Garton, A. Naylor, A.D. Rawlings, B.P. Slingsby, D.G. Smith, A.K. Takle, R.W. Ward, 6-Aryl-pyrazolo[3,4-b]pyridines: potent inhibitors of glycogen synthase kinase-3 (GSK-3), Bioorg. Med. Chem. Lett. 13 (2003) 3055–3057, https://doi.org/10.1016/S0960-894X(03)00645-0.

[2] L.W. Mohamed, M.A. Shaaban, A.F. Zaher, S.M. Alhamaky, A.M. Elsahar, Synthesis of new pyrazoles and pyrozolo [3,4-b] pyridines as anti-inflammatory agents by inhibition of COX-2 enzyme, Bioorg. Chem. 83 (2019) 47–54, https://doi.org/10.1016/j.bioorg.2018.10.014.

[3] R. Menegatti, G.M.S. Silva, G. Zapata-Sudo, J.M. Raimundo, R.T. Sudo, E.J. Barreiro, C.A.M. Fraga, Design, synthesis, and pharmacological evaluation of new neuroactive pyrazolo[3,4-b]pyrrolo[3,4-d]pyridine derivatives with in vivo hypnotic and analgesic profile, Bioorg. Med. Chem. 14 (2006) 632–640, https://doi.org/10.1016/j.bmc.2005.08.042.

[4] S. Eagon, J.T. Hammill, M. Sigal, K.J. Ahn, J.E. Tryhorn, G. Koch, B. Belanger, C.A. Chaplan, L. Loop, A.S. Kashtanova, K. Yniguez, H. Lazaro, S.P. Wilkinson, A. L. Rice, M.O. Falade, R. Takahashi, K. Kim, A. Cheung, C. DiBernardo, J.J. Kimball, E.A. Winzeler, K. Eribez, N. Mittal, F.-J. Gamo, B. Crespo, A. Churchyard, I. García-Barbazán, J. Baum, M.O. Anderson, B. Laleu, R.K. Guy, Synthesis and structure–Activity relationship of dual-stage antimalarial pyrazolo[3,4- *b*] pyridines, J. Med. Chem. 63 (2020) 11902–11919, https://doi.org/10.1021/acs.jmedchem.0c01152.

[5] L. Urquhart, FDA new drug approvals in Q1 2021, Nat. Rev. Drug Discov. 20 (2021), https://doi.org/10.1038/d41573-021-00067-x, 334–334.

[6] A. Donaire-Arias, A.M. Montagut, R. Puig de la Bellacasa, R. Estrada-Tejedor, J. Teixidó, J.I. Borrell, 1H-Pyrazolo[3,4-b]pyridines: synthesis and biomedical applications, Molecules 27 (2022) 2237, https://doi.org/10.3390/molecules27072237.

[7] J. Orrego-Hernández, C. Lizarazo, J. Cobo, J. Portilla, Pyrazolo-fused 4-azafluorenones as key reagents for the synthesis of fluorescent dicyanovinylidene-substituted derivatives, RSC Adv. 9 (2019) 27318–27323, https://doi.org/10.1039/C9RA04682H.

[8] R. Qiu, S. Qiao, B. Peng, J. Long, G. Yin, A mild method for the synthesis of bis-pyrazolo[3,4-b:4′,3′-e]pyridine derivatives, Tetrahedron Lett. 59 (2018) 3884–3888, https://doi.org/10.1016/j.tetlet.2018.09.033.

[9] V.P. Vidali, G. Nigianni, G.D. Athanassopoulou, A. Canko, B. Mavroidi, D. Matiadis, M. Pelecanou, M. Sagnou, Synthesis of novel pyrazolo[3,4-b]pyridines with affinity for β-amyloid plaques, Molbank 2022 (2022) M1343, https://doi.org/10.3390/M1343.

[10] M. García, I. Romero, J. Portilla, Synthesis of Fluorescent 1,7-Dipyridyl-bis-pyrazolo[3,4- b :4′,3′- e]pyridines: Design of Reversible Chemosensors for Nanomolar Detection of Cu 2+, ACS Omega 4 (2019) 6757–6768, https://doi.org/10.1021/acsomega.9b00226.

[11] U. Krishnan, S. Manickam, S.K. Iyer, BF3 detection by pyrazolo-pyridine based fluorescent probe and applications in bioimaging and paper strip analysis, J. Mol. Liq. 385 (2023) 122413, https://doi.org/10.1016/j.molliq.2023.122413.

[12] E. Polo, K. Ferrer-Pertuz, J. Trilleras, J. Quiroga, M. Gutiérrez, Microwave-assisted one-pot synthesis in water of carbonylpyrazolo[3,4-: B] pyridine derivatives catalyzed by $InCl_3$and sonochemical assisted condensation with aldehydes to obtain new chalcone derivatives containing the pyrazolopyridinic moiety, RSC Adv. 7 (2017), https://doi.org/10.1039/c7ra10127a.

[13] A. Simay, K. Takacs, L. Toth, ChemInform Abstract:Aminopyrazoles. II. synthesis of pyrazolo(3,4,-b)pyridines via vilsmeier-haack reaction of 5-acetaminopyrazoles, Chem. Informationsd 13 (1982), https://doi.org/10.1002/chin.198224238.

[14] A.D. Becke, Density-functional thermochemistry. III. The role of exact exchange, J. Chem. Phys. 98 (1993) 5648–5652, https://doi.org/10.1063/1.464913.

[15] A.J. Cohen, N.C. Handy, Dynamic correlation, Mol. Phys. 99 (2001) 607–615, https://doi.org/10.1080/00268970010023435.

[16] A.D. McLean, G.S. Chandler, Contracted Gaussian basis sets for molecular calculations. I. Second row atoms, Z =11–18, J. Chem. Phys. 72 (1980) 5639–5648, https://doi.org/10.1063/1.438980.

[17] R. Krishnan, J.S. Binkley, R. Seeger, J.A. Pople, Self-consistent molecular orbital methods. XX. A basis set for correlated wave functions, J. Chem. Phys. 72 (1980) 650–654, https://doi.org/10.1063/1.438955.

[18] M.J. Frisch, J.A. Pople, J.S. Binkley, Self-consistent molecular orbital methods 25. Supplementary functions for Gaussian basis sets, J. Chem. Phys. 80 (1984) 3265–3269, https://doi.org/10.1063/1.447079.

[19] T. Yanai, D.P. Tew, N.C. Handy, A new hybrid exchange–correlation functional using the Coulomb-attenuating method (CAM-B3LYP), Chem. Phys. Lett. 393 (2004) 51–57, https://doi.org/10.1016/j.cplett.2004.06.011.

[20] T.H. Dunning, Gaussian basis sets for use in correlated molecular calculations. I. The atoms boron through neon and hydrogen, J. Chem. Phys. 90 (1989) 1007–1023, https://doi.org/10.1063/1.456153.

[21] S. Miertuš, E. Scrocco, J. Tomasi, Electrostatic interaction of a solute with a continuum. A direct utilizaion of AB initio molecular potentials for the prevision of solvent effects, Chem. Phys. 55 (1981) 117–129, https://doi.org/10.1016/0301-0104(81)85090-2.

[22] S. Miertus, J. Tomasi, Approximate evaluations of the electrostatic free energy and internal energy changes in solution processes, Chem. Phys. 65 (1982) 239–245, https://doi.org/10.1016/0301-0104(82)85072-6.

[23] J.L. Pascual-ahuir, E. Silla, I. Tuñon, GEPOL: an improved description of molecular surfaces. III. A new algorithm for the computation of a solvent-excluding surface, J. Comput. Chem. 15 (1994) 1127–1138, https://doi.org/10.1002/jcc.540151009.

[24] F. London, Théorie quantique des courants interatomiques dans les combinaisons aromatiques, J. Phys. Radium 8 (1937) 397–409, https://doi.org/10.1051/jphysrad:01937008010039700.

[25] R. McWeeny, Perturbation theory for the fock-Dirac density matrix, Phys. Rev. 126 (1962) 1028–1034, https://doi.org/10.1103/PhysRev.126.1028.

[26] R. Ditchfield, Self-consistent perturbation theory of diamagnetism, Mol. Phys. 27 (1974) 789–807, https://doi.org/10.1080/00268977400100711.

[27] J. Vasić, D. Dimić, M. Antonijević, E.H. Avdović, D. Milenković, Đ. Nakarada, J. Dimitrić Marković, M. Molnar, M. Lončarić, D. Bešlo, Z. Marković, The electronic effects of 3-methoxycarbonylcoumarin substituents on spectral, antioxidant, and protein binding properties, Int. J. Mol. Sci. 24 (2023) 11820, https://doi.org/10.3390/ijms241411820.

[28] D.S. Dimić, G.N. Kaluđerović, E.H. Avdović, D.A. Milenković, M.N. Živanović, I. Potočňák, E. Samoľová, M.S. Dimitrijević, L. Saso, Z.S. Marković, J.M. Dimitrić Marković, Synthesis, crystallographic, quantum chemical, antitumor, and molecular docking/dynamic studies of 4-hydroxycoumarin-neurotransmitter derivatives, Int. J. Mol. Sci. 23 (2022) 1001, https://doi.org/10.3390/ijms23021001.

[29] P. Jeeva, S. Sudha, A. Rakić, D. Dimić, D. Ramarajan, D. Barathi, Structural, spectroscopic, quantum chemical, and molecular docking study towards cartilage protein of (3E,3′E)-3,3′-(1,4-phenylenebis(azanediyl))bis(cyclohex-2-en-1-one), J. Mol. Struct. 1274 (2023) 134429, https://doi.org/10.1016/j.molstruc.2022.134429.

[30] D. Dimić, D. Milenković, J. Ilić, B. Šmit, A. Amić, Z. Marković, J. Dimitrić Marković, Experimental and theoretical elucidation of structural and antioxidant properties of vanillylmandelic acid and its carboxylate anion, Spectrochim. Acta Part A Mol. Biomol. Spectrosc. 198 (2018) 61–70, https://doi.org/10.1016/j.saa.2018.02.063.

[31] C. Beatrice Vicentini, A. Cesare Veronese, P. Giori, B. Lumachi, M. Guarneri, A new general and efficient synthesis of imidazo[4,5-c]pyrazole derivatives, Tetrahedron 46 (1990) 5777–5788, https://doi.org/10.1016/S0040-4020(01)87774-7.

[32] O. Meth-Cohn, B. Narine, B. Tarnowski, A versatile new synthesis of quinolines and related fused pyridines. Part 7. The conversion of acetamidothiophens into thienopyridines, J. Chem. Soc. Perkin Trans. 1 (1981) 1531, https://doi.org/10.1039/p19810001531.